NASA TECHNICAL REPORT

NASA TR R-279

NASA TR R-279

PLASTIC BEHAVIOR OF CIRCULAR PLATES UNDER TRANSVERSE IMPULSE LOADINGS OF GAUSSIAN DISTRIBUTION

by Robert G. Thomson

Langley Research Center
Langley Station, Hampton, Va.

NATIONAL AERONAUTICS AND SPACE ADMINISTRATION • WASHINGTON, D. C. • JANUARY 1968

NASA TR R-279

PLASTIC BEHAVIOR OF CIRCULAR PLATES UNDER TRANSVERSE IMPULSE LOADINGS OF GAUSSIAN DISTRIBUTION

By Robert G. Thomson

Langley Research Center
Langley Station, Hampton, Va.

NATIONAL AERONAUTICS AND SPACE ADMINISTRATION

For sale by the Clearinghouse for Federal Scientific and Technical Information
Springfield, Virginia 22151 – CFSTI price $3.00

PLASTIC BEHAVIOR OF CIRCULAR PLATES UNDER TRANSVERSE IMPULSE LOADINGS OF GAUSSIAN DISTRIBUTION*

By Robert G. Thomson
Langley Research Center

SUMMARY

An analytical study of the plastic response of a circular plate of uniform thickness subjected to a normal axisymmetric impulse of Gaussian distribution is presented. The Gaussian impulse loading is assumed initially to impart a momentum to the plate. The plate is thereafter prescribed as free from external loads. The kinetic energy of motion is assumed to be dissipated in plastic deformation. The radial and circumferential strain and strain-rate distributions of the plastically deforming plate are determined as a function of time and space from derived deflection expressions. Only the bending action of the plate is taken into account and the plate material is assumed to behave as a perfectly plastic-rigid continuum.

The possibility of a fracture or separation of the plate material occurring during deformation is discussed. Maximum values of strain and strain rate are shown to occur in the circumferential components, and a mode of failure by radial fractures is indicated.

INTRODUCTION

The impingement and fracture of the main wall of a space vehicle by meteoroids are of major concern to the spacecraft designer. Protective devices, such as meteoroid bumpers, have been proposed to shatter the impinging meteoroid and to lessen its penetrating potential. It has been shown both theoretically and experimentally (refs. 1 and 2) that the resulting cloud of meteoroid and bumper debris passes on to the main wall of the space vehicle as an impulsive loading having a general Gaussian distribution. A study of the dynamic response of a plate under this impulsive type loading could well classify the mode or manner of fracture at failure recently observed experimentally on double sheet models of a bumper and main wall configuration. (See refs. 3 and 4.)

*The information presented herein was included in a thesis submitted in partial fulfillment of the requirements for the degree of Doctor of Philosophy, Virginia Polytechnic Institute, Blacksburg, Va., 1966.

A thorough analysis of the behavior of an impulsively loaded plate should include not only the plastic but also the elastic response of the plate material. Because of the complex time-dependent properties of the problem, however, most analyses consider only the rigid-plastic response of the plate and neglect its elastic behavior entirely. This rigid-plastic assumption for plate behavior is adopted in the present paper. The energy dissipation process then becomes one of pure plastic deformation in which a plate, once given an initial kinetic energy of motion, dissipates energy in plastic deformation and acquires a permanently deformed shape when the motion terminates. Energy transformation due to rotary inertia and dissipation due to transverse shear displacements are neglected.

The existing analyses of the dynamic rigid-plastic behavior of plates consider the loading function as constant over the loaded area (refs. 5 to 9). Although this assumption on loading simplifies the mathematical development of the problem, it greatly restricts its application. The present analysis, therefore, considers a more general representation of the loading function. The loading is still considered to be axisymmetric with respect to the center of the plate, but its radial distribution is given a general Gaussian shape.

SYMBOLS

$a = \frac{1}{\sqrt{2}S}$

b	radius of finite circular plate
C	constant of integration (see eq. (17))
$2h$	plate thickness
$\dot{k}_r$	radial curvature rate
$\dot{k}_\theta$	circumferential curvature rate
M_o	yield-moment resultant, $\sigma_o h^2$; maximum bending moment plate can sustain
M_r	radial bending-moment resultant
M_θ	circumferential bending-moment resultant

q load distribution

Q_r transverse shear stress resultant

r, θ, z radial, circumferential, and axial plate coordinates, respectively (see fig. 2)

S standard deviation

t time

t^* time of cessation of all plate motion after impact

t_1 time at which hinge-circle radius has decreased to zero

$V = \dot{w}(r,t)$

$V_o = \dot{w}(0,0)$

w plate deflection in transverse direction (z-direction)

w^* permanent plate deflection for $t \geq t^*$

$\epsilon_r, \epsilon_\theta$ radial and circumferential strain, respectively

$\delta(t)$ Dirac δ–function, $\int_{-\infty}^{\infty} \delta(t)\, dt = 1$

μ mass per unit area of plate material

$\rho(t)$ radius of hinge circle

$\rho(0)$ initial position of hinge circle at $t = 0$

σ_{ij} stress components

$\sigma_r, \sigma_\theta, \sigma_z$ principal radial, circumferential, and transverse stress, respectively

σ_o yield stress in simple tension or compression (assumed to be identical in magnitude)

$\phi(t)$ function of time (see eq. (32))

A dot over a symbol indicates partial differentiation with respect to time t.

FUNDAMENTAL CONCEPTS

General Considerations

The present analysis determines the rigid-plastic bending deformations, strains, and strain rates experienced by a circular plate when subjected to an axisymmetric Gaussian impulse loading. The circular plate, of radius b, is taken to be simply supported, uniform in thickness, and composed of a plate material that is incompressible, ideally plastic (no work-hardening), and isotropic in yielding. Only the bending action of the plate is taken into account and the elastic deformations as well as the membrane forces are neglected. The plate material behavior is therefore considered to be perfectly plastic-rigid and is assumed to deform according to the Tresca yield condition and the associated flow rule.

The structural loading on the plate is assumed to result from a momentum exchange with an axisymmetric momentum impulse having a general radial Gaussian distribution where S is the standard deviation of the Gaussian momentum distribution. (See fig. 1.) This momentum exchange can be considered as an impulse loading such that at t = 0, a Gaussian distribution of load is instantaneously imparted to the entire plate. Thereafter, the plate is considered to be free from external loads.

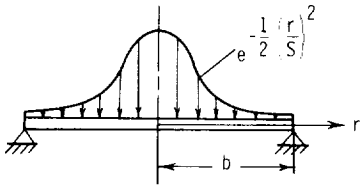

Figure 1.- Momentum distribution.

Equation of Motion

Let r, θ, and z be a cylindrical coordinate system whose origin is located at the center of the undeformed middle surface of the circular plate and whose Z-axis is pointing vertically downward. (See fig. 2.) It follows from the symmetry of loading that the only nonvanishing stresses are σ_r and σ_θ and the transverse shear force Q_r. Integration of σ_r and σ_θ through the thickness of the plate leads to the moments M_r and M_θ.

The forces and moments acting on an element of the plate middle surface are then as shown in figure 2. Positive directions of the bending moments and shearing forces are shown, and all stress resultants are specified per unit length of line element of the middle surface of the plate. Summation of the vertical forces and summation of the moments acting on the plate result in the following equation of motion:

$$\frac{\partial}{\partial r}(rM_r) = M_\theta + \int_0^r (\mu\ddot{w} - q)r\,dr \tag{1}$$

where the loading q is prescribed by

$$q = \mu V_o e^{-a^2r^2}\delta(t)$$

and where the plate is initially at rest but immediately upon impact assumes a velocity distribution. In addition, the simply supported boundary conditions are

$$w(b,t) = M_r(b,t) = 0 \tag{2}$$

The stress profile through the thickness of a plate in rigid-plastic theory is different from that postulated in the bending of an elastic plate. If the rigid-plastic plate is to bend, each horizontal layer through the plate thickness must be at the yield condition. This assumption, for the Tresca yield condition, creates a discontinuity of stress at the middle surface which is allowable within the framework of plastic-rigid theory (ref. 10). The resulting principal moments (employing Tresca's yield condition) are thus written as

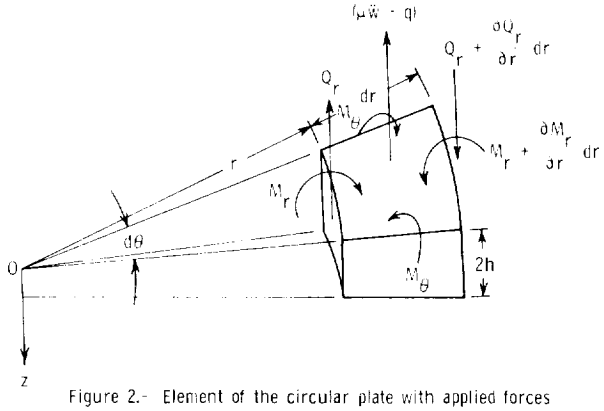

Figure 2.- Element of the circular plate with applied forces and moments.

$$\left.\begin{aligned} M_r &= \sigma_r h^2 \\ M_\theta &= \sigma_\theta h^2 \end{aligned}\right\} \tag{3}$$

where $2h$ is the plate thickness, and σ_r and σ_θ are positive constants for positive values of z. Hence, the yield moment M_o equals $\sigma_o h^2$, where σ_o is the yield stress in simple tension or compression.

Strain-Displacement Relations

The customary linear strain-displacement relations for strain are retained and particles originally on a normal to the plate middle surface are considered to remain normal to the middle surface as the plate is bent. The rates of radial and circumferential straining for the present axisymmetric problem can then be written as

$$\dot{\epsilon}_r = -z \frac{\partial^2 \dot{w}}{\partial r^2} = z\dot{k}_r \tag{4}$$

$$\dot{\epsilon}_\theta = -z \frac{1}{r} \frac{\partial \dot{w}}{\partial r} = z\dot{k}_\theta \tag{5}$$

where $\dot{k}_r$ and $\dot{k}_\theta$ are the radial and circumferential curvature rates, respectively. Consequently,

$$\frac{\dot{\epsilon}_r}{\dot{\epsilon}_\theta} = \frac{\dot{k}_r}{\dot{k}_\theta} \tag{6}$$

Plasticity Relations

The idealized perfectly plastic-rigid response of the plate material is characterized by a constitutive equation. The dependence between the plastic strain-rate components $\dot{\epsilon}^p_{ij}$ and the stress components σ_{ij} is formulated according to the flow (or incremental) theory of plasticity. (See ref. 11.) For the case of ideal plasticity, the strain-rate components $\dot{\epsilon}^p_{ij}$ are expressed simply as

$$\dot{\epsilon}^p_{ij} = G \frac{\partial f}{\partial \sigma_{ij}} \qquad (i,j = 1,2,3)$$

where

f yield function which depends only on stress state

G scalar function depending, in general, on spatial coordinates and time; G determines magnitude of plastic strain rates

For ideal plasticity the plastic strain-rate components $\dot{\epsilon}^p_{ij}$ are directed normal (outward direction positive) to the yield surface, $f(\sigma_{ij})$ being constant. The yield surface considered in this paper is that corresponding to the criteria of Tresca. It is concluded from the Tresca yield condition that yielding occurs when the maximum shear stress reaches a certain value or, mathematically, when

$$\sigma_1 - \sigma_3 = \sigma_0$$

where σ_1, σ_2, and σ_3 are the principal stresses and $\sigma_1 \geq \sigma_2 \geq \sigma_3$. Tresca's yield condition for this problem is shown graphically in figure 3 in a σ_r, σ_θ plane ($\sigma_z = 0$).

The plastic strain-rate components lie normal to the yield surface except at the corners of the hexagon where the normal is not defined but is bounded by the normals to the intersecting adjacent straight sides. The Tresca yield hexagon, therefore, not only defines the relationship between σ_r and σ_θ but also characterizes the flow mechanisms (or curvature rates) of deformation. (See refs. 5, 10, and 12.)

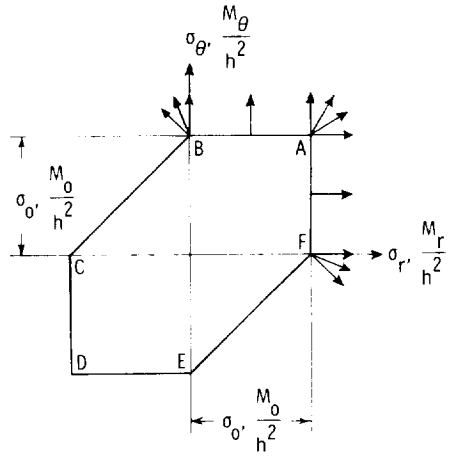

Figure 3.- Tresca yield hexagon.

For a simply supported circular plate and the type of loading considered in this paper, the plate cannot reach the flow limit without first becoming plastic at the center; hence, through symmetry, $M_r = M_\theta = M_o$ at $r = 0$. At the simply supported edge of the plate, the moment M_r must vanish, or $M_r = 0$ at $r = b$. The two plastic regimes of Tresca's yield hexagon satisfying these boundary conditions and the equation of motion (eq. (1)) are regimes (point) A and (line) AB (fig. 3). Thus, the plate is initially divided into two different plastic regimes; an inner central plastic regime (called regime A) in which

$$\left.\begin{aligned} M_r &= M_\theta = M_o \\ \dot{k}_r &\geqq 0 \\ \dot{k}_\theta &\geqq 0 \end{aligned}\right\} \tag{7}$$

and a second outer annulus (called regime AB) in which

$$\left.\begin{aligned} 0 \leqq M_r &\leqq M_o \\ M_\theta &= M_o \\ \dot{k}_r &= 0 \\ \dot{k}_\theta &\geqq 0 \end{aligned}\right\} \tag{8}$$

where $\dot{k}_r$ and $\dot{k}_\theta$ are the radial and circumferential curvature rates defined in equations (4) and (5). Note that in the outer annulus, the restriction of zero radial curvature

rate (eq. (8)) establishes, at most, a linear relationship in r for the velocity in that regime. For the velocities considered, the entire plate is in a plastic condition when deformation commences.

Deformation Modes

At the interface between the plastic regimes A and AB, a hinge circle is formed (as indicated in fig. 4) because of a discontinuity in the rate of circumferential curvature $\dot{k}_\theta$ between the two regimes. (See ref. 5.) It will be found subsequently that this hinge circle will have a maximum radius at $t = 0$ when the kinetic energy imparted to the plate is a maximum, and will decrease thereafter and move toward the center of the plate. When the hinge circle finally shrinks to zero, the plate motion does not cease, but the plate continues to deform in such a manner that an inverted cone is formed with the hinge at $r = 0$, until the velocity becomes zero everywhere.

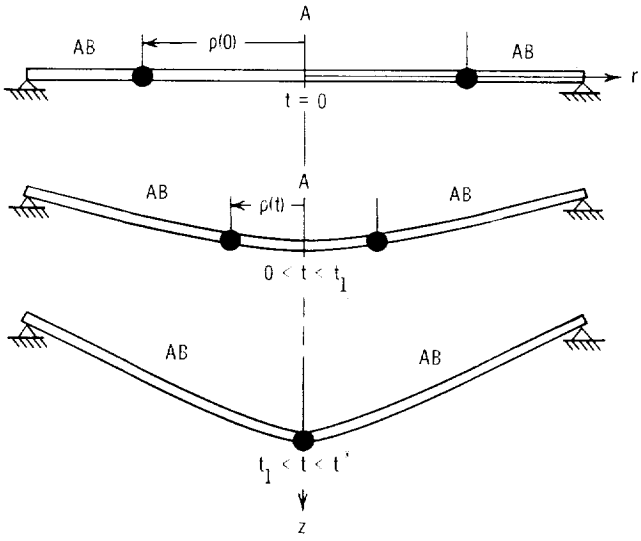

Figure 4.- Mode of deformation.

Certain higher order derivatives, when passing through the hinge circle, are found to be discontinuous according to the plasticity theory developed for the dynamics of plastic circular plates. (For details, see refs. 5, 8, and 13.) Since the deflection $w(r,t)$ obviously must remain continuous across a hinge circle,

$$\left[\frac{dw}{dt}\right] = 0 = \left[\dot{w}\right] + \dot{\rho}\left[\frac{\partial w}{\partial r}\right] \tag{9}$$

where the brackets denote possible discontinuities in the enclosed quantities in passing through the hinge circle and $\dot{\rho}$ is the rate of change of the hinge circle with time. The velocity of the plate particles $\dot{w}$ and the slope of the plate $\partial w/\partial r$ must remain continuous for moving hinge circles. The following continuity expressions can also be shown to be continuous across $r = \rho(t)$ even though they are composed of members (that is, $\partial^2 w/\partial r^2$, $\ddot{w}$, and $\partial \dot{w}/\partial r$) which may be discontinuous:

$$\left[\frac{\partial \dot{w}}{\partial r}\right] + \dot{\rho}\left[\frac{\partial^2 w}{\partial r^2}\right] = 0 \tag{10}$$

$$\left[\ddot{w}\right] + \dot{\rho}\left[\frac{\partial \dot{w}}{\partial r}\right] = 0 \tag{11}$$

Although equations (10) and (11) are not used directly to obtain a solution for $w(r,t)$, they are employed as a check on the validity of the radial and circumferential strain and strain rates derived from $w(r,t)$.

MATHEMATICAL ANALYSIS

The analytical derivation of the deflection of the plastically deforming plate is divided into two sections. The first section presents the solution for the motion of the plate when the plate is divided into two distinct plasticity regimes, separated by a hinge circle, up to the time of the disappearance of this hinge circle. The second section contains the solution for the motion of the plate as it continues to deform, up to the time of cessation of all motion. From the deflection expressions, the velocities, strains, and strain rates can be determined and are evaluated in the appendix.

Solution With Hinge Circle of Finite Radius

Velocity determination.- For a perfectly plastic-rigid circular plate initially subjected to a general Gaussian distribution of momentum, the resulting velocity distributions are as follows:

In regime A, the expression for velocity is obtained by direct integration of equation (1) with respect to time, it being noted that M_r and M_θ are both equal to M_o (eq. (7)),

$$\dot{w} = V_o e^{-a^2 r^2} \qquad (0 \leqq r \leqq \rho(t)) \tag{12}$$

Note also from equation (12) that the curvature rates $\dot{k}_r$ and $\dot{k}_\theta$, in regime A, are non-negative (eq. (7)).

In regime AB, however, the determination of the proper velocity distribution is not as straightforward. The first condition that can be utilized is that the radial curvature rate $\dot{k}_r$ must be zero (eq. (8)) and thus, the velocity has at most a linear dependence in r. The velocity must be continuous across the hinge circle, and from the boundary condition of zero displacement at the simply supported edge (eq. (2)), must have zero velocity at the simply supported edge. The satisfaction of these conditions leads to the following expression for the velocity distribution in regime AB:

$$\dot{w} = V_o e^{-a^2[\rho(t)]^2}\left[\frac{b - r}{b - \rho(t)}\right] \qquad (\rho(t) \leqq r \leqq b) \qquad (13)$$

where $\rho(t)$ is the radius of the hinge circle which is, as yet, undetermined.

The equation of motion (eq. (1)) is therefore not uniquely satisfied in regime AB until $\rho(t)$ is determined as a function of t. In order to solve for the proper time variation of $\rho(t)$, the equation of motion is utilized, together with the velocity expression (eq. (13)) and the associated boundary conditions for regime AB

$$\left.\begin{aligned} M_r(\rho,t) &= M_o \\ M_r(b,t) &= 0 \end{aligned}\right\} \qquad (14)$$

where $0 \leqq M_r \leqq M_o$ for $\rho \leqq r \leqq b$.

Equation (13) is differentiated to obtain the following expression for the acceleration:

$$\ddot{w} = V_o e^{-a^2\rho^2}\frac{b - r}{(b - \rho)^2}\left(1 - 2a^2b\rho + 2a^2\rho^2\right)\dot{\rho} \qquad (15)$$

which is substituted into equation (1) with M_θ set equal to M_o $(t > 0)$. Integration of equation (1) then determines an expression in $M_r(r,t)$. Applying the boundary conditions on M_r (eq. (14)) determines the constant of integration and leads to the following first-order total differential equation in $\rho(t)$:

$$\frac{12M_o}{\mu V_o b^2}\,dt = \frac{e^{-a^2\rho^2}}{b}\left(1 - 2a^2b\rho + 2a^2\rho^2\right)\left[-1 - 2\frac{\rho}{b} + 3\left(\frac{\rho}{b}\right)^2\right]d\rho \qquad (16)$$

Equation (16), when integrated, yields (from ref. 14)

$$\frac{12M_o}{\mu V_o b^2}t + C = \left[-1 + \frac{6}{(ab)^2}\left(1 - \frac{\rho}{b}\right) - \frac{\rho}{b} + 5\left(\frac{\rho}{b}\right)^2 - 3\left(\frac{\rho}{b}\right)^3\right]e^{-a^2\rho^2} + \frac{3\sqrt{\pi}}{(ab)^3}\,\mathrm{erf}(a\rho) \qquad (17)$$

The constant of integration C can be evaluated in terms of $\rho(0)$, the initial location of the hinge circle. Thus for $t = 0$ and $\rho(t) = \rho(0)$, C becomes

$$C = \left[-1 + \frac{6}{(ab)^2}\left(1 - \frac{\rho(0)}{b}\right) - \frac{\rho(0)}{b} + 5\left(\frac{\rho(0)}{b}\right)^2 - 3\left(\frac{\rho(0)}{b}\right)^3\right]e^{-a^2\rho(0)^2} + \frac{3\sqrt{\pi}}{(ab)^3}\,\mathrm{erf}(a\rho(0)) \qquad (18)$$

The initial location of the hinge circle radius $\rho(0)$ is determined from two requirements: (1) that the time rates of curvature $\dot{k}_r, \dot{k}_\theta$ be nonnegative in regime A and (2) that $d\rho/dt$ (eq. (16)) be negative (since the kinetic energy imparted to the plate is a maximum at $t = 0$ and decreases thereafter). Also, of course, the value determined for $\rho(0)$ must be unique. The value of $\rho(0)$ satisfying these requirements is found to depend on the shape of the initial Gaussian momentum distribution. For a Gaussian distribution that resembles a localized load $\left(ab > \sqrt{2}\right)$, it is found that the requirement that $d\rho/dt$ be negative governs the determination of $\rho(0)$. Hence, solving equation (16) for the maximum value of $\rho(0)/b$ that will still yield negative values of $d\rho/dt$ results in

$$\frac{\rho(0)}{b} = \frac{1 - \sqrt{1 - \frac{2}{(ab)^2}}}{2} \qquad \left(2 \leqq \sqrt{2}ab < \infty\right) \tag{19}$$

For a Gaussian distribution that resembles a more distributed load $\left(ab < \sqrt{2}\right)$, the governing criteria for the determination of $\rho(0)$ is that the rate of curvature be nonnegative in regime A and also that the value of $\rho(0)$ be unique. Thus, from equations (4) and (12) the rate of radial curvature $\dot{k}_r$ can be written as

$$\dot{k}_r = -\frac{\partial^2 \dot{w}}{\partial r^2} = 2V_o a^2 \left(1 - 2a^2r^2\right) e^{-a^2r^2} \tag{20}$$

and for $\dot{k}_r$ to remain nonnegative at $r = \rho(0)$ and for $\rho(0)$ to be unique for all values of ab, $\rho(0)/b$ must be equal to

$$\frac{\rho(0)}{b} = \frac{S}{b} = \frac{1}{\sqrt{2}ab} \qquad \left(1 \leqq \sqrt{2}ab \leqq 2\right) \tag{21}$$

The lower limit on ab $\left(ab = 1/\sqrt{2}\right)$ places the hinge circle at the outer edge of the plate.

For values of $ab < 1/\sqrt{2}$, the hinge circle remains at the outer edge of the plate since the boundary condition $M_r(b,t) = 0$ (from eq. (2)) prohibits regime A from encompassing the edge of the plate and passing beyond. Hence, for $ab < 1/\sqrt{2}$,

$$\frac{\rho(0)}{b} = 1 \qquad \left(0 < \sqrt{2}ab \leqq 1\right) \tag{22}$$

The lower limit on ab may only approach zero since the integral evaluation of equation (17) is invalid when $a = 0$. However, solutions do exist in the neighborhood of zero and are sufficient for practical application. The lower limit on ab $(ab \to 0)$ represents a uniformly distributed impulse over the entire plate.

The value of t at the time the hinge circle vanishes, or $t = t_1$, can be determined from equation (17) by setting $\frac{\rho}{b} = 0$ to yield

$$\frac{12M_o}{\mu V_o b^2} t_1 = -1 + \frac{6}{(ab)^2} - C = -1 + \frac{6}{(ab)^2} + \left[1 - \frac{6}{(ab)^2}\left(1 - \frac{\rho(0)}{b}\right) + \frac{\rho(0)}{b} - 5\left(\frac{\rho(0)}{b}\right)^2 + 3\left(\frac{\rho(0)}{b}\right)^3\right] e^{-a^2\rho(0)^2} - \frac{3\sqrt{\pi}}{(ab)^3} \operatorname{erf}(a\rho(0)) \tag{23}$$

The expression for t_1 is a cubic in ab and is plotted as a function of $\frac{12M_o}{V_o b^2 \mu} t_1$ in figure 5. As is shown in figure 5, different expressions for $\rho(0)/b$ are used in the

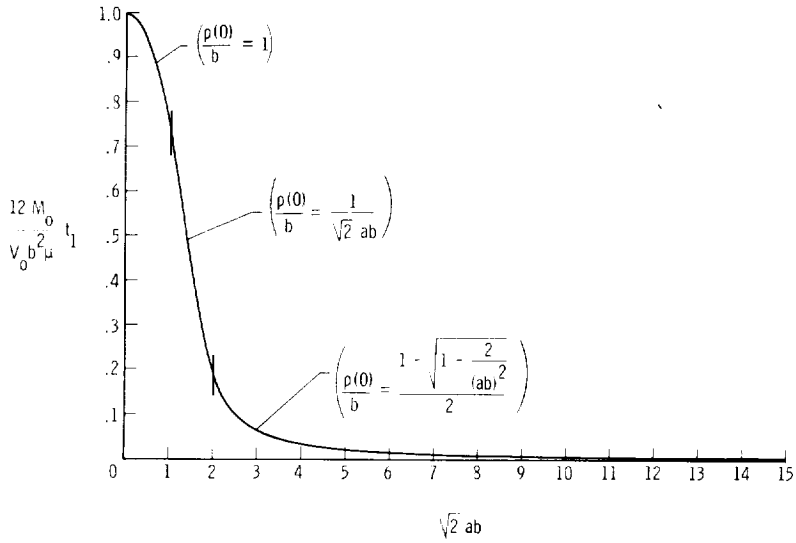

Figure 5.- Time interval t_1 for initial hinge-circle radius to decrease to zero as a function of initial Gaussian distribution parameter ab.

three different ranges of ab. (See eqs. (19), (21), and (22).) Note that as ab approaches ∞, $\frac{12M_o}{\mu V_o b^2} t_1$ approaches 0 and as ab approaches 0, $\frac{12M_o}{\mu V_o b^2} t_1$ approaches 1; this value corresponds to the value for $\frac{12M_o}{\mu V_o b^2} t_1$ presented in reference 6 for a uniformly distributed impulse.

Deflection.- The deflection of the plate can now be determined since the velocities of deformation have been established. The plate, during deformation, is divided into three distinct regions of interest as shown in figure 6.

For elements of the plate located between the outer edge of the plate and the initial position of the hinge-circle radius ($\rho(0)$), or in region I of figure 6, the deflection expression is dependent only on the velocity as given for the plastic regime AB (eq. (13)) and can be written as

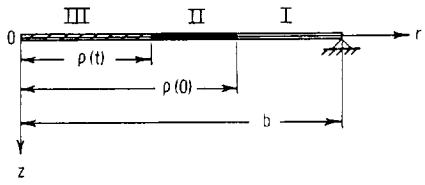

Figure 6.- Hinge circle and plasticity regimes.

$$w(r,t) = V_o \int_0^t e^{-a^2\rho^2}\left(\frac{b - r}{b - \rho}\right)dt \qquad (\rho(0) \leq r \leq b) \qquad (24)$$

In region II of figure 6, elements of the plastic plate are first located in the plastic regime A and then as the hinge-circle radius passes over, in the plastic regime AB. The deflection is therefore dependent not only on the motion due to the velocity of the regime A when the point in question was in regime A, but also after the time $t(r)$ (when the hinge circle passes through that point of $\rho = r$) on the deflection due to the velocity present in regime AB at that point up to the time t.

$$w(r,t) = V_o e^{-a^2r^2}t(r) + V_o \int_{t(r)}^t e^{-a^2\rho^2}\left(\frac{b - r}{b - \rho}\right)dt \qquad (\rho(t) \leq r \leq \rho(0)) \qquad (25)$$

In region III, the elements of the plate are always situated in the plastic regime A. The deflection is therefore dependent only on the velocity present in regime A (eq. (12)) and can be written

$$w(r,t) = V_o e^{-a^2r^2}t \qquad (0 \leq r \leq \rho(t)) \qquad (26)$$

Expressing dt in terms of $d\rho$ (eq. (17)) and integrating equations (24) and (25) yield (from ref. 14)

$$w(r,t) = V_o \frac{\mu V_o b^2}{12M_o}\left(1 - \frac{r}{b}\right)\left\{\left[\frac{3}{2}\left(\frac{\rho}{b}\right)^2 + \frac{3}{2(ab)^2} - \frac{1}{2} - \frac{\rho}{b}\right]e^{-2a^2\rho^2} - \left[\frac{3}{2}\left(\frac{\rho(0)}{b}\right)^2 + \frac{3}{2(ab)^2} - \frac{1}{2} - \frac{\rho(0)}{b}\right]e^{-2a^2\rho(0)^2}\right\} \qquad (\rho(0) \leq r \leq b) \qquad (27)$$

$$w(r,t) = V_o e^{-a^2r^2} t(r) + V_o \frac{\mu V_o b^2}{12M_o}\left(1 - \frac{r}{b}\right)\left\{\left[\frac{3}{2}\left(\frac{\rho}{b}\right)^2 + \frac{3}{2(ab)^2} - \frac{1}{2} - \frac{\rho}{b}\right]e^{-2a^2\rho^2} - \left[\frac{3}{2}\left(\frac{r}{b}\right)^2 + \frac{3}{2(ab)^2} - \frac{1}{2} - \frac{r}{b}\right]e^{-2a^2r^2}\right\} \qquad (\rho \leq r \leq \rho(0)) \qquad (28)$$

where $t(r)$ is found from equation (17).

For $t(r)$, ρ/b in equation (17) is replaced by r/b, because $t(r)$ is the time it takes for the hinge circle to pass through the point $\rho = r$. Thus $t(r)$, from equations (17), (18), and (23) can be written as

$$\frac{12M_o}{\mu V_o b^2} t(r) = 1 - \frac{6}{(ab)^2} + \left[-1 + \frac{6}{(ab)^2}\left(1 - \frac{r}{b}\right) - \frac{r}{b} + 5\left(\frac{r}{b}\right)^2 - 3\left(\frac{r}{b}\right)^3\right]e^{-a^2r^2} + \frac{3\sqrt{\pi}}{(ab)^3}\,\mathrm{erf}(ar) + \frac{12M_o}{\mu V_o b^2} t_1 \qquad (29)$$

The time the hinge circle vanishes t_1 is given by equation (23) and $\rho(0)/b$ is defined over different ranges of ab by equations (19), (21), and (22).

Solution With Hinge Circle of Zero Radius

When the hinge-circle radius shrinks to zero at $t = t_1$ and the entire plate is in the plastic regime AB, the previous analysis must be terminated because the acceleration vanishes and the equation of motion reduces to (see (eq. (1))

$$\frac{\partial}{\partial r}(rM_r) = M_o \qquad (30)$$

or

$$M_r = M_o + \frac{C_3}{r} \qquad (31)$$

Since $M_r = M_o$ at $r = 0$, C_3 is zero and M_r remains at the constant yield moment value of M_o for all radial values; this result is in contradiction to the prescribed plasticity condition in regime AB (see eq. (8)) and the simply supported edge condition (eq. (2)).

Since the entire plate is now in the plastic regime AB, except for the origin, the radial curvature rate (eq. (4)) is zero. Integration of the radial-curvature-rate expression, while the boundary condition of zero deflection at $r = b$ and the continuity

conditions on the deflection and velocity at $t = t_1$ are maintained, yields the following expression for the plate deflection:

$$w(r,t) = \phi(t)\left(1 - \frac{r}{b}\right) + w\left(r,t_1\right) \qquad \left(t \geq t_1\right) \tag{32}$$

where $w\left(r,t_1\right)$ is the deflection at $t = t_1$, given by equations (27) and (28) with ρ set equal to zero, and where $\phi(t)$ is an arbitrary function. The plasticity condition of zero radial-curvature rate is satisfied if $\frac{d\phi(t)}{dt} \geq 0$. This condition on $\phi(t)$ is examined for its validity once $\phi(t)$ has been determined. Note, however, that the slope of the deflection as given by equation (32) is not zero at $r = 0$, because of the zero radial-curvature-rate condition.

By a procedure similar to that used in the previous section of the paper, the acceleration is obtained by differentiation of equation (32) and is substituted into equation (1) with $M_\theta = M_o$. The subsequent integration of equation (1) and application of the boundary conditions

$$\left.\begin{aligned} M_r &= M_o \qquad (r = 0) \\ M_r &= 0 \qquad (r = b) \end{aligned}\right\} \tag{33}$$

yield

$$\ddot{\phi} = -\frac{12M_o}{\mu b^2} \tag{34}$$

which upon integration, by utilizing the conditions evaluated at $t = t_1$

$$\left.\begin{aligned} \phi\left(t_1\right) &= 0 \\ \dot{\phi}\left(t_1\right) &= V_o \end{aligned}\right\} \tag{35}$$

becomes

$$\phi(t) = -\frac{6M_o}{\mu b^2}\left(t - t_1\right)^2 + V_o\left(t - t_1\right) \tag{36}$$

It can be seen from equation (36) that $\dot{\phi}$ is indeed greater than or equal to zero, and $w(r,t)$ for $t > t_1$ can be written as

$$w(r,t) = w(r,t_1) + \left(1 - \frac{r}{b}\right)\left[-\frac{6M_o}{\mu b^2}(t - t_1)^2 + V_o(t - t_1)\right] \tag{37}$$

The time $t = t^*$ at which the entire plate comes to rest can be found by differentiating equation (37) to obtain the velocity, by equating this expression for velocity to zero, and by solving for t^*. Hence,

$$\frac{12M_o}{\mu V_o b^2} t^* = 1 + \frac{12M_o}{\mu V_o b^2} t_1 \tag{38}$$

and the permanent deflection shape, denoted as $w^*(r,t^*)$ for $t = t^*$, can then be written as

$$w^*(r,t^*) = w(r,t_1) + \left(1 - \frac{r}{b}\right)\frac{\mu b^2 V_o}{12M_o}\frac{V_o}{2} \tag{39}$$

The complete time-dependent expressions for the deflection shape of the plastically deforming plate, beginning with the initiation of motion, continuing past the time $t = t_1$ (the vanishing of the hinge circle), and continuing up to the time of cessation of all plate motion $t = t^*$ have thus been determined. The complete time-dependent strains and strain rates of the plastically deforming plate can then be determined and are so derived in the appendix.

RESULTS AND DISCUSSION

In the evaluation of the permanently deformed shape of the plastic plate as the velocity drops to zero, it has been tacitly assumed that the plate remains continuous and homogeneous. In reality, however, "separation" or "fracture" of the plate material could occur, under certain loading conditions, if the plate experiences "critical" strain or strain rates or combinations of these over portions of its surface. Under these conditions, of course, the application of the analysis should be terminated. After a choice of criteria is made, the knowledge of the complete time-dependent strain rate, strain, and velocity histories experienced by the Gaussian impacted plate permits the analyst to determine whether the integrity of the plate material has been maintained. In addition, a study of the strain and strain rate distributions can indicate the manner or mode of separation or fracture of the plate material when failure does occur. For these reasons, two sample Gaussian impulse loadings have been considered, and the velocity, strain rate, and strain distributions have been determined at various times after impact. Radial distributions of the velocities, strain rates, and strains are plotted for the two sample loadings in figures 7 to 11.

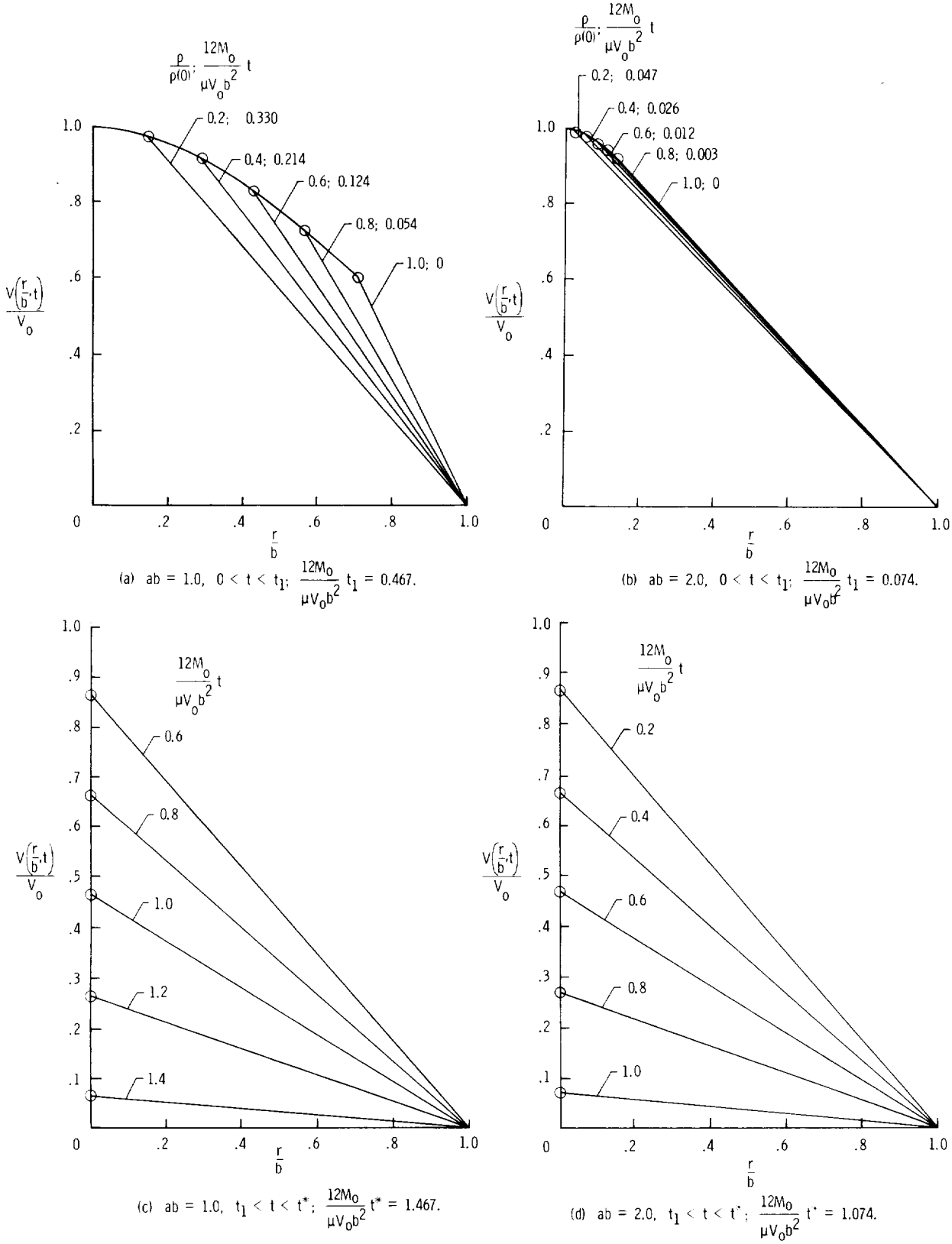

(a) ab = 1.0, $0 < t < t_1$; $\frac{12M_o}{\mu V_o b^2} t_1 = 0.467$.

(b) ab = 2.0, $0 < t < t_1$; $\frac{12M_o}{\mu V_o b^2} t_1 = 0.074$.

(c) ab = 1.0, $t_1 < t < t^*$; $\frac{12M_o}{\mu V_o b^2} t^* = 1.467$.

(d) ab = 2.0, $t_1 < t < t^*$; $\frac{12M_o}{\mu V_o b^2} t^* = 1.074$.

Figure 7.- History of radial velocity distribution for two sample loadings.

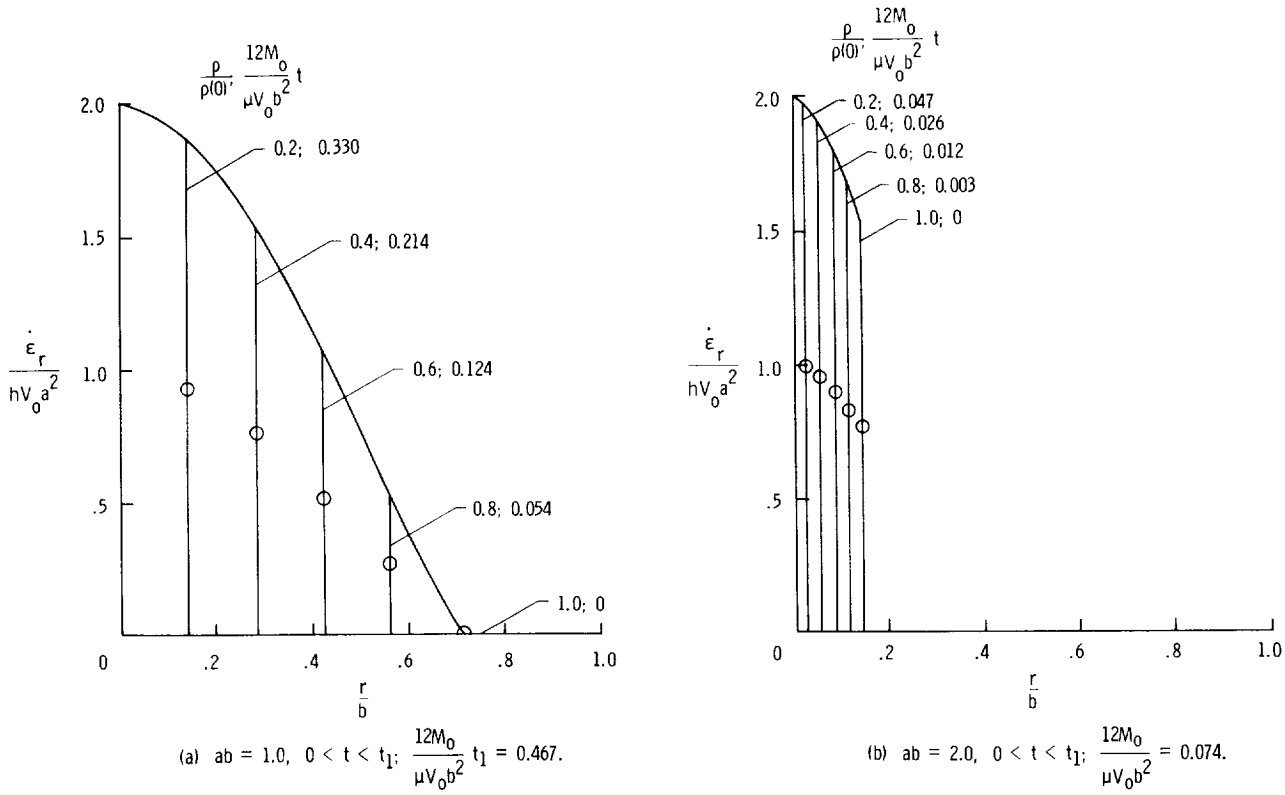

(a) ab = 1.0, $0 < t < t_1$; $\frac{12M_0}{\mu V_0 b^2} t_1 = 0.467$.

(b) ab = 2.0, $0 < t < t_1$; $\frac{12M_0}{\mu V_0 b^2} = 0.074$.

Figure 8.- History of radial strain rate for two sample loadings. Radial strain rate is zero after hinge circle vanishes. $t > t_1$.

In parts (a) and (b) of figures 7 to 11 the times chosen range between $t = 0$ and $t = t_1$, during which time interval the hinge circle has a finite radius. The specific location of the hinge radius for the particular times chosen $\left(\frac{\rho}{\rho(0)} = 1, 0.8, 0.6, 0.4, \text{and } 0.2\right)$ is indicated in the figures by a circle. In parts (c) and (d) of figures 7, 9, 10, and 11 the times chosen range between $t = t_1$ and $t = t^*$. In this time interval, the hinge circle has already shrunk to zero radius; thus, the plate is entirely within the plastic regime AB. Parts (a) and (c) are calculated by using a value of ab of 1.0 and parts (b) and (d) are calculated by using a value of ab of 2.0. These sample values of ab (that is, Gaussian shape parameters) were chosen to fall within different ranges of ab for which different expressions are valid for $\rho(0)/b$. (See fig. 5.)

Velocities

The velocities are shown plotted in figure 7. The velocity as shown in parts (a) and (b) exhibits Gaussian character in the central region of the plate and decreases linearly with increasing radius in the surrounding annulus. The central region is seen to decrease progressively as time increases (ρ decreasing) until the entire plate is within the plastic regime AB and the velocity is completely linear in character. The velocity as represented by parts (c) and (d) of figure 7 remains linear, the magnitudes

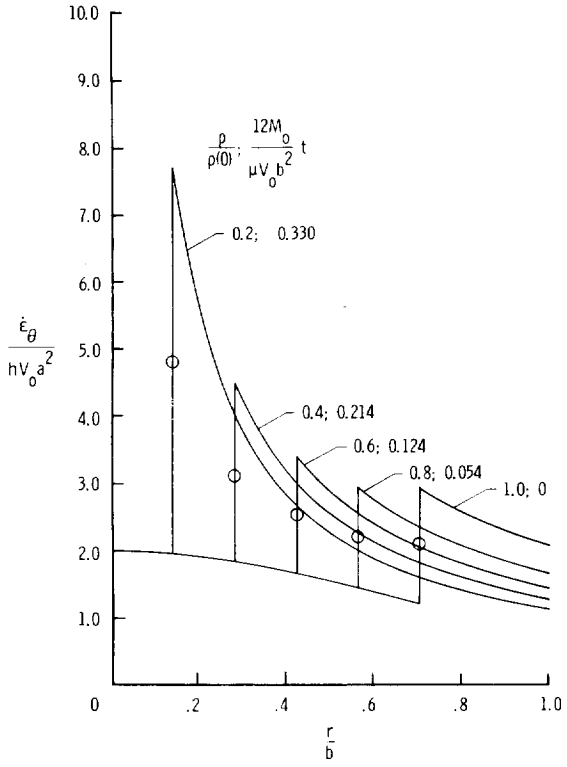

(a) ab = 1.0, $0 < t < t_1$; $\frac{12M_0}{\mu V_0 b^2} t_1 = 0.467$.

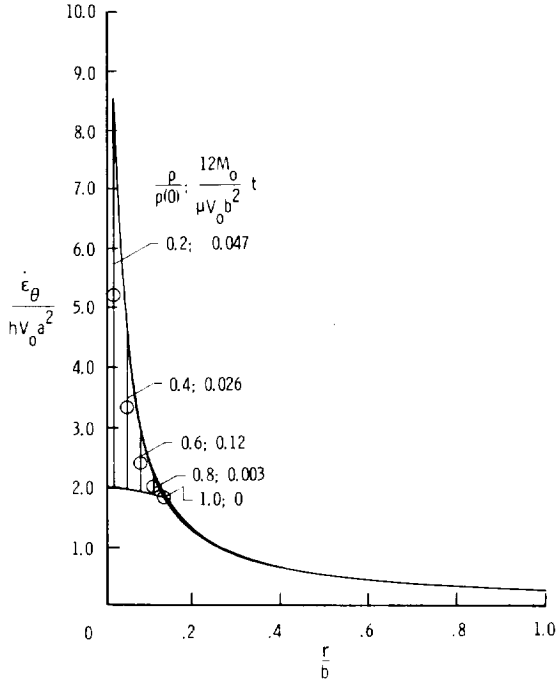

(b) ab = 2.0, $0 < t < t_1$; $\frac{12M_0}{\mu V_0 b^2} t_1 = 0.074$.

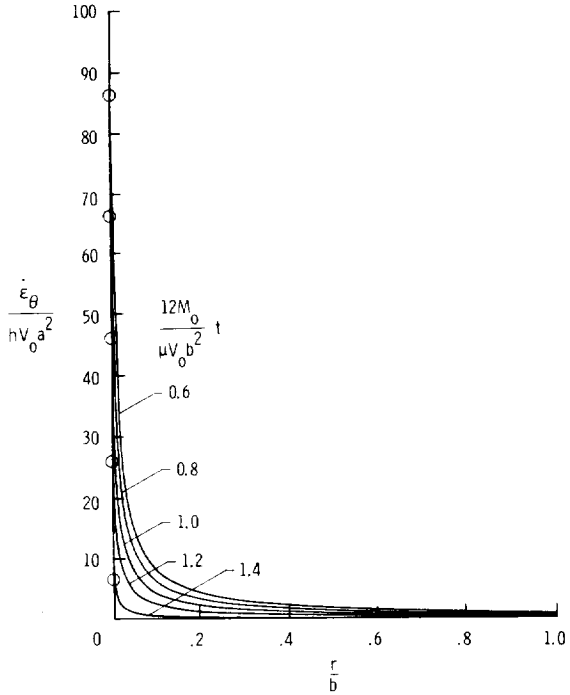

(c) ab = 1.0, $t_1 < t < t^*$; $\frac{12M_0}{\mu V_0 b^2} t^* = 1.467$.

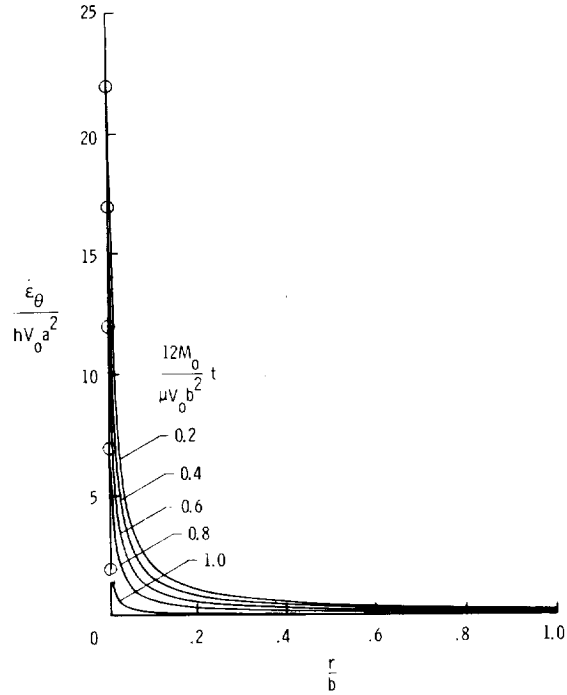

(d) ab = 2.0, $t_1 < t < t^*$; $\frac{12M_0}{\mu V_0 b^2} t^* = 1.074$.

Figure 9.- History of circumferential strain rate for two sample loadings.

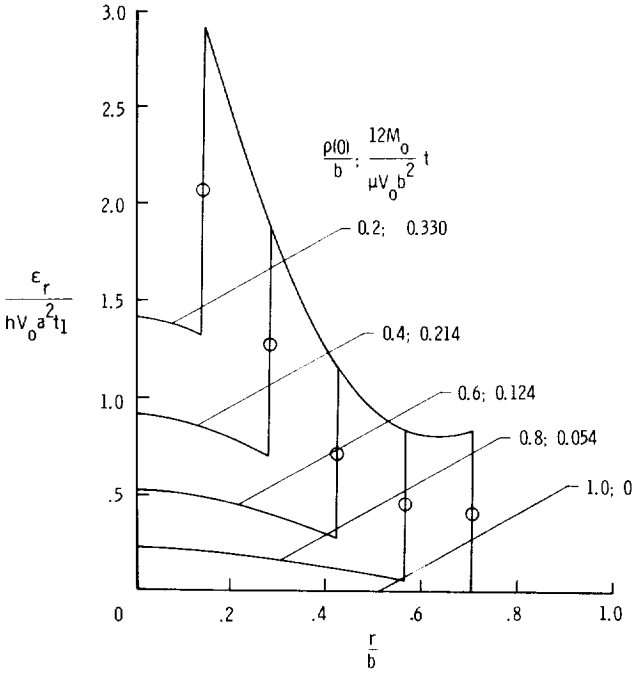

(a) ab = 1.0, $0 < t < t_1$; $\frac{12M_o}{\mu V_o b^2} t_1 = 0.467$.

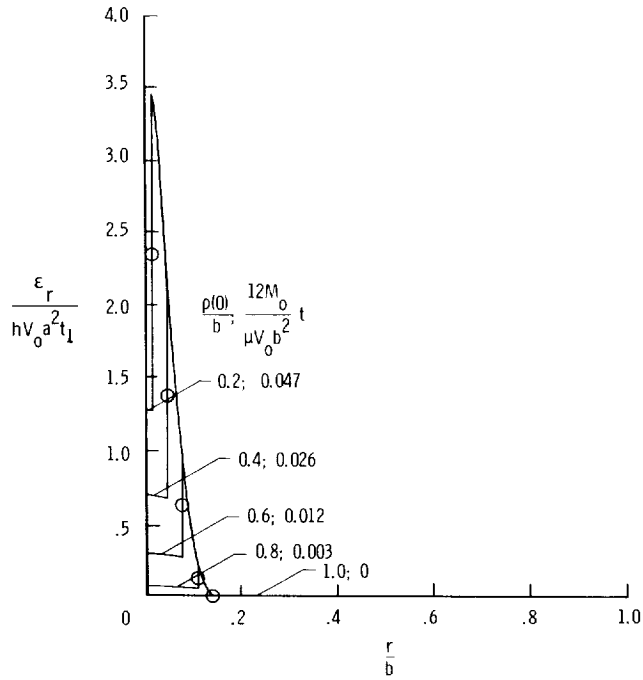

(b) ab = 2.0, $0 < t < t_1$; $\frac{12M_o}{\mu V_o b^2} t_1 = 0.074$.

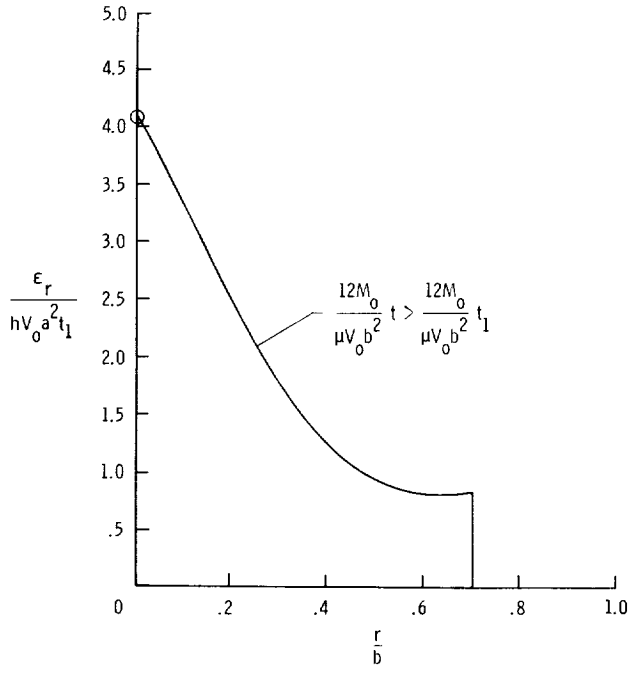

(c) ab = 1.0, $t_1 < t < t^*$; $\frac{12M_o}{\mu V_o b^2} t^* = 1.467$.

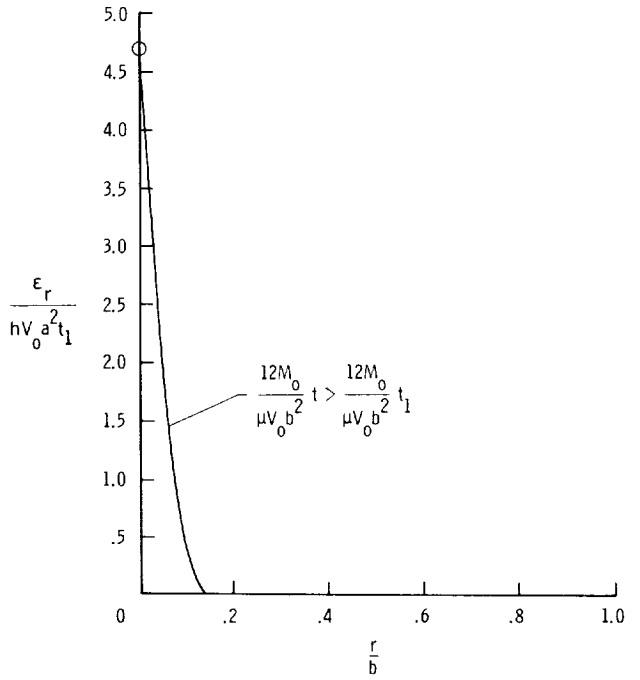

(d) ab = 2.0, $t_1 < t < t^*$; $\frac{12M_o}{\mu V_o b^2} t^* = 1.074$.

Figure 10.- History of radial strain for two sample loadings.

decreasing as the time increases. These velocity profiles are as expected, since the basic plasticity assumptions made with respect to the rates of curvature only admit of these profiles in the two plastic regimes (eqs. (12) and (13)).

Radial Strain Rate

The radial strain rates are plotted in figure 8. The radial strain rates are zero in plastic regime AB because of the basic plasticity assumption made with regard to the rates of curvature possible in this regime (see eqs. (4) and (8)) and indeed the radial strain rate (as given by eqs. (A6) and (A18)) is zero for all times. In figures 8(a) and 8(b) the radial strain rate possesses an approximate Gaussian radial distribution in the central region of the plate (regime A) with a discontinuous decrease to zero across the hinge circle to the surrounding annulus of regime AB. Note that the strain rate does not vary with time but the movement of the hinge circle toward the center of the plate decreases the central plastic region (regime A) and causes a decrease in the percentage of the plastic plate with nonzero radial strain rate. The magnitude of the discontinuity present at the hinge circle, however, increases with decreasing hinge radius.

Circumferential Strain Rate

The circumferential strain rates are plotted in figure 9. In parts (a) and (b) of figure 9, the circumferential strain rates also exhibit a Gaussian radial distribution of the central region (plastic regime A) of the plastic plate; however, a large increase in magnitude occurs as one passes into the surrounding annulus of regime AB. The circumferential strain rate in regime AB is the maximum value of strain rate experienced by the plastically deforming plate. The circumferential strain rates in regime AB are inversely proportional to the radius and decrease accordingly as the radius increases. The magnitude of the discontinuity across the hinge circle is similarly seen to increase as the radius of the hinge circle decreases. In parts (c) and (d) of figure 9, the entire plate is contained within the plastic regime AB and the circumferential rates are shown to decrease in magnitude with increasing time with a radial distribution again proportional to the inverse of the radius.

Radial Strain

The radial strains are shown plotted in figure 10. The central region of the plastic plate exhibits an approximate Gaussian type radial distribution of radial strain (plastic regime A) with a discontinuous "jump" in strain developing across the moving hinge circle in passing into the plastic regime AB. This discontinuity in radial strain at the moving hinge circle is the jump condition noted in equation (10) for $\partial^2 w/\partial r^2$ (divided by -h); a second discontinuity develops at $\frac{r}{b} = \frac{\rho(0)}{b}$ for $\frac{\rho(0)}{b} = \frac{1}{\sqrt{2}ab}$ (fig. 10(a)), but not

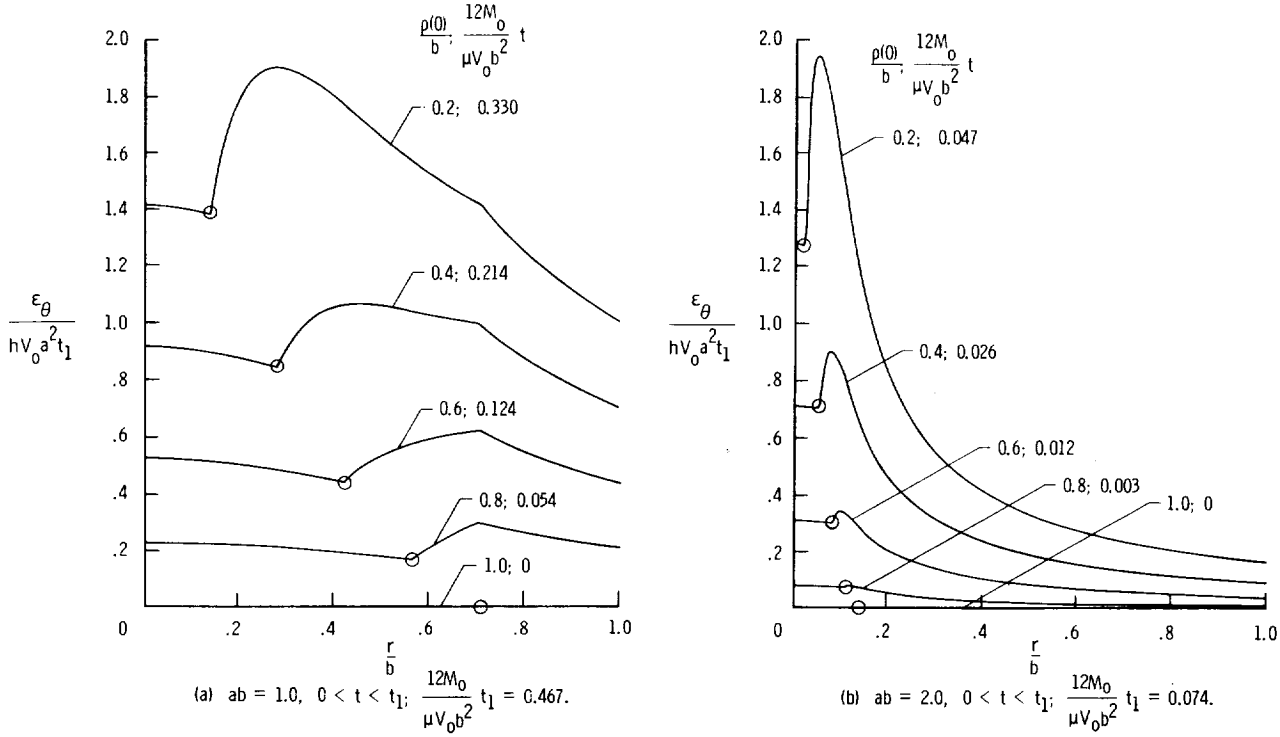

(a) ab = 1.0, $0 < t < t_1$; $\frac{12M_0}{\mu V_0 b^2} t_1 = 0.467$.

(b) ab = 2.0, $0 < t < t_1$; $\frac{12M_0}{\mu V_0 b^2} t_1 = 0.074$.

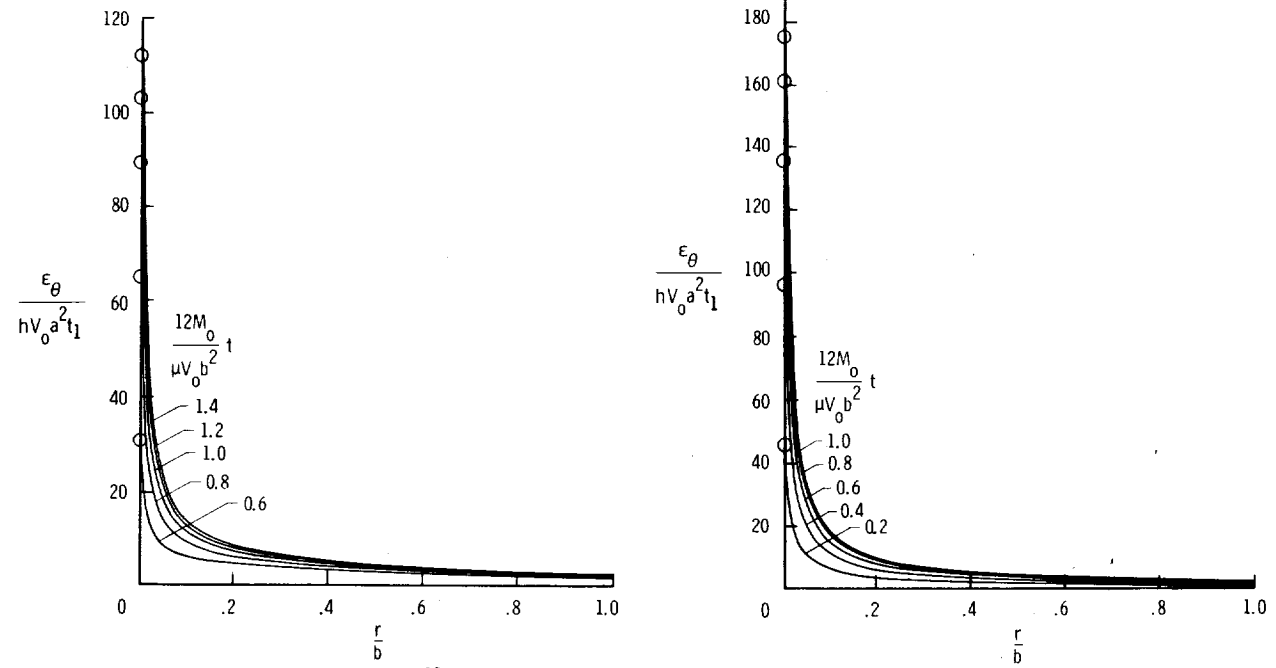

(c) ab = 1.0, $t_1 < t < t^*$; $\frac{12M_0}{\mu V_0 b^2} t^* = 1.467$.

(d) ab = 2.0, $t_1 < t < t^*$; $\frac{12M_0}{\mu V_0 b^2} t^* = 1.074$.

Figure 11.- History of circumferential strain for two sample loadings.

for $\frac{\rho(0)}{b} = \frac{1}{2}\left[1 - \sqrt{1 - \frac{2}{(ab)^2}}\right]$ (fig. 10(b)). The plastic regime AB always has zero radial strain. For regime A, however, as the hinge circle moves toward the center of the plate, this central plastic region decreases and the surrounding annulus of regime AB encompasses regions of the plate formerly situated in regime A. This annulus thus contains residual strains from regime A, as well as the radial straining that occurs across the discontinuity of the moving hinge circle as is shown in parts (a) and (b) of figure 10. As is to be expected, the radial strains begin at zero and increase in magnitude as the time progresses. In parts (c) and (d) of figure 10, the residual radial strains present in the plastic regime AB (caused by radial straining in the plastic regime A and radial straining at the discontinuity of the hinge circle) remain constant with time, for $t > t_1$, and no further increase in radial strain occurs because the radial straining in regime AB is zero.

Circumferential Strain

The circumferential strains are plotted in figure 11. In parts (a) and (b) of figure 11, the circumferential strains again exhibit Gaussian radial distribution in the inner central region (plastic regime A), a discontinuity developing in the slope of the circumferential strain as one passes through the moving hinge circle into the surrounding annulus. In the surrounding annulus, the magnitudes of the circumferential strains increase since this region contains both residual strains developed when this part of the plate was in the plastic regime A and further circumferential straining when this part passes into the plastic regime AB. A second discontinuity in slope occurs when the initial position of the hinge circle is reached if the initial position is determined from $\frac{\rho(0)}{b} = \frac{1}{\sqrt{2}ab}$. (See fig. 11(a).) The circumferential strains begin at zero and increase in magnitude as the time increases. In parts (c) and (d) of figure 11, the residual circumferential strains developed in regimes A and AB are present (and remain constant with respect to time) and additional circumferential straining is experienced by the plate (now completely in regime AB) as time progresses. The circumferential strain continues to increase in magnitude as time progresses and reaches a maximum as the impacted plate comes to rest. (Note again that in the immediate neighborhood of $r = 0$, the solutions presented are invalid.)

The increase in magnitude of the circumferential strains and strain rates as one passes from the central region (plastic regime A) of the plate to the surrounding annulus (plastic regime AB) could have a special significance. With the passing of time, the hinge circle decreases in radius, as has been noted before, and the circumferential strain rates and strains in the plasticity regime AB immediately adjacent to the hinge circle subsequently increase in magnitude. This increase in the magnitude of the

circumferential strain rate and strain eventually exceeds that of their radial counterparts as the hinge-circle radius shrinks to zero. If failure by fracture or separation does occur during the deformation process, the magnitudes of the circumferential components probably would be the maximum values of strain rate and strain experienced by the plate at failure, and fracture would occur along radial paths.

CONCLUDING REMARKS

An exact analytical solution is presented for the plastic behavior of a circular plate subjected to a general radial Gaussian impulse loading. Axial symmetry being assumed, a small deflection bending analysis is developed to determine the complete time-dependent strain and strain-rate distributions present in the plastically deforming plate from the moment of impact (considered to be instantaneous) to the cessation of motion. Graphical representations of the radial and circumferential components of the strain and strain rate are presented for various times between initial impact and cessation.

A study of these graphical representations indicates that the maximum values of strain rate occur in the circumferential direction and that the radial strains exhibit a discontinuity in crossing through the moving hinge circle which separates the deforming plate into two distinct plasticity regimes. The maximum values of strain and strain rate are also shown to be distributed initially in annular rings about the center of the plate. These maximum values increase in magnitude as time progresses, and the hinge circle moves toward the center of the plate. The circumferential components eventually increase to become the maximum values in both strain and strain rate experienced by the plate.

A study of these strain and strain-rate distributions suggests a pattern of fracture of the plate material when failure occurs. Because the circumferential strains and strain rates are higher than their radial counterparts, fractures can be expected to occur along radial lines. These radial fractures may initiate the catastrophic petalling-type failure noted experimentally on the inner wall of double-sheet micrometeoroid protective devices.

Langley Research Center,
National Aeronautics and Space Administration,
Langley Station, Hampton, Va., May 22, 1967,
124-08-01-13-23.

APPENDIX

VELOCITIES, STRAIN RATES, AND STRAINS OF THE PLASTICALLY DEFORMING PLATE

The complete time-dependent expressions for the deflection shape of the plastically deforming plate have been determined in the body of the paper. In this appendix, the complete time-dependent velocities, strain rates, and strains are derived.

Solutions for Times Prior to Shrinking of Hinge Circle to Zero Radius

Velocities.- The velocities are as given in equations (12) and (13) or can be derived by differentiation of equations (24) to (26) with respect to t, $t(r)$ being considered constant with respect to time,

$$\dot{w}(r,t) = V_o e^{-a^2 r^2} \qquad (0 \leqq r \leqq \rho) \qquad (A1)$$

$$\dot{w}(r,t) = V_o e^{-a^2 \rho^2} \frac{b - r}{b - \rho} \qquad (\rho \leqq r \leqq b) \qquad (A2)$$

Strain rates.- The strain rates, as given by equations (4) and (5), are linear in z, the maximum strain rate occurring at $z = \pm h$. Consider the maximum strain rate in tension for a positive bending moment ($z = h$) (from eqs. (4) and (5)):

$$\dot{\epsilon}_r = -h \frac{\partial^2 \dot{w}(r,t)}{\partial r^2} \qquad (A3)$$

$$\dot{\epsilon}_\theta = -\frac{h}{r} \frac{\partial \dot{w}(r,t)}{\partial r} \qquad (A4)$$

Differentiation of equations (A1) and (A2) with respect to r accordingly yields for the radial strain rate

$$\dot{\epsilon}_r = 2hV_o a^2 e^{-a^2 r^2} \left[1 - 2(ab)^2 \left(\frac{r}{b}\right)^2\right] \qquad (0 \leqq r \leqq \rho) \qquad (A5)$$

$$\dot{\epsilon}_r = 0 \qquad (\rho \leqq r \leqq b) \qquad (A6)$$

and for the circumferential strain rate

$$\dot{\epsilon}_\theta = 2hV_o a^2 e^{-a^2 r^2} \qquad (0 \leqq r \leqq \rho) \qquad (A7)$$

$$\dot{\epsilon}_\theta = \frac{h}{br} V_o e^{-a^2 \rho^2} \frac{1}{1 - \frac{\rho}{b}} \qquad (\rho \leqq r \leqq b) \qquad (A8)$$

Strains.- The maximum strain in tension for a positive bending moment (z = h) from equations (A3) and (A4) can be written as

$$\epsilon_r = -h \frac{\partial^2 w(r,t)}{\partial r^2} \qquad (A9)$$

$$\epsilon_\theta = -\frac{h}{r} \frac{\partial w(r,t)}{\partial r} \qquad (A10)$$

Differentiation of equations (24) to (26) with respect to r, accordingly, yields for the radial strain

$$\epsilon_r(r,t) = 2ha^2 V_o e^{-a^2 r^2} \left[1 - 2(ab)^2 \left(\frac{r}{b}\right)^2\right] t \qquad (0 \leqq r \leqq \rho) \qquad (A11)$$

$$\epsilon_r(r,t) = 2ha^2 V_o e^{-a^2 r^2} \left[1 - 2(ab)^2 \left(\frac{r}{b}\right)^2\right] t(r) + \frac{h}{b^2} \frac{\mu V_o b^2}{12 M_o} e^{-2a^2 r^2} \left[1 - 2(ab)^2 \frac{r}{b} + 2(ab)^2 \left(\frac{r}{b}\right)^2\right]^2 \left(1 + 3\frac{r}{b}\right) \qquad (\rho \leqq r \leqq \rho(0)) \qquad (A12)$$

$$\epsilon_r(r,t) = 0 \qquad (\rho(0) \leqq r \leqq b) \qquad (A13)$$

Note that t is the time when the hinge circle reaches the radial position r and that t(r) is the time the hinge circle crosses the point $\rho = r$. (See eq. (29).) Similarly, differentiation of equations (24) to (26) with respect to r for the circumferential strain yields

$$\epsilon_\theta(r,t) = 2hV_o a^2 e^{-a^2 r^2} t \qquad (0 \leqq r \leqq \rho) \qquad (A14)$$

APPENDIX

$$\epsilon_\theta(r,t) = 2hV_o a^2 e^{-a^2r^2} t(r) + \frac{V_o h}{b^2 \frac{r}{b}} \frac{\mu V_o b^2}{12M_o} \left\{ \left[\frac{3}{2}\left(\frac{\rho}{b}\right)^2 + \frac{3}{2(ab)^2} - \frac{1}{2} - \frac{\rho}{b} \right] e^{-2a^2\rho^2} \right.$$

$$\left. - \left[\frac{3}{2}\left(\frac{r}{b}\right)^2 + \frac{3}{2(ab)^2} - \frac{1}{2} - \frac{r}{b} \right] e^{-2a^2r^2} \right\} \qquad (\rho \leq r \leq \rho(0)) \qquad \text{(A15)}$$

$$\epsilon_\theta(r,t) = \frac{V_o h}{b^2 \frac{r}{b}} \frac{\mu V_o b^2}{12M_o} \left\{ \left[\frac{3}{2}\left(\frac{\rho}{b}\right)^2 + \frac{3}{2(ab)^2} - \frac{1}{2} - \frac{\rho}{b} \right] e^{-2a^2\rho^2} \right.$$

$$\left. - \left[\frac{3}{2}\left(\frac{\rho(0)}{b}\right)^2 + \frac{3}{2(ab)^2} - \frac{1}{2} - \frac{\rho(0)}{b} \right] e^{-2a^2\rho(0)^2} \right\} \qquad (\rho(0) \leq r \leq b) \qquad \text{(A16)}$$

Solutions for Times After Disappearance of Hinge Circle

The velocities, strain rates, and strains for $t_1 \leq t \leq t^*$ can be obtained by the use of equation (37).

Velocities.- Differentiation of equation (37) with respect to t yields

$$\dot{w}(r,t) = V_o(b - r)\left[\frac{12M_o}{\mu V_o b^2}(t_1 - t) + 1\right] \qquad (0 \leq r \leq b) \qquad \text{(A17)}$$

Strain rates.- The maximum strain rates in tension as found from equations (A3) and (A4), by differentiation with respect to r of equation (37), become

$$\dot{\epsilon}_r = 0 \qquad (0 \leq r \leq b) \qquad \text{(A18)}$$

$$\dot{\epsilon}_\theta = \frac{hV_o}{b^2 \frac{r}{b}}\left[\frac{12M_o}{\mu V_o b^2}(t_1 - t) + 1\right] \qquad (0 < r \leq b) \qquad \text{(A19)}$$

Strains.- The maximum strains in tension for a positive bending moment ($z = h$) are found from equations (A9) and (A10) by the proper differentiation of equation (37) with respect to r, and can be written as follows:

APPENDIX

$$\frac{\epsilon_r(r,t)}{hV_o a^2 t_1} = 2e^{-a^2r^2}\left[1 - 2(ab)^2\left(\frac{r}{b}\right)^2\right]\frac{t(r)}{t_1} + \frac{e^{-2a^2r^2}}{(ab)^2}\frac{V_o \mu b^2}{12M_o t_1}\left\{\left[1 - 2(ab)^2\frac{r}{b} + 2(ab)^2\left(\frac{r}{b}\right)^2\right]^2\left(1 + 3\frac{r}{b}\right)\right\} \qquad (0 \leq r \leq \rho(0)) \qquad \text{(A20)}$$

$$\frac{\epsilon_r(r,t)}{hV_o a^2 t_1} = 0 \qquad (\rho(0) \leq r \leq b) \qquad \text{(A21)}$$

$$\frac{\epsilon_\theta(r,t)}{hV_o a^2 t_1} = 2e^{-a^2r^2}\frac{t(r)}{t_1} + \frac{1}{(ab)^2\frac{r}{b}}\frac{V_o b^2}{12M_o t_1}\left\{\frac{3}{2(ab)^2} - \frac{1}{2} - \left[\frac{3}{2(ab)^2} - \frac{1}{2} + \frac{3}{2}\left(\frac{r}{b}\right)^2 - \frac{r}{b}\right]e^{-2a^2r^2}\right\}$$
$$+ \frac{1}{(ab)^2\frac{r}{b}}\left[-\frac{6M_o}{\mu V_o b^2}\frac{(t - t_1)^2}{t_1} + \frac{t}{t_1} - 1\right] \qquad (0 < r \leq \rho(0)) \qquad \text{(A22)}$$

$$\frac{\epsilon_\theta(r,t)}{hV_o a^2 t_1} = \frac{1}{(ab)^2\frac{r}{b}}\frac{\mu V_o b^2}{12M_o t_1}\left\{\frac{3}{2(ab)^2} - \frac{1}{2} - \left[\frac{3}{2}\left(\frac{\rho(0)}{b}\right)^2 + \frac{3}{2(ab)^2} - \frac{1}{2} - \frac{\rho(0)}{b}\right]e^{-2a^2\rho(0)^2}\right\}$$
$$+ \frac{1}{(ab)^2\frac{r}{b}}\left[-\frac{6M_o}{\mu V_o b^2}\frac{(t - t_1)^2}{t_1} + \frac{t}{t_1} - 1\right] \qquad (\rho(0) \leq r \leq b) \qquad \text{(A23)}$$

Note that in the neighborhood of $\frac{r}{b} = 0$, equations (A8), (A15), (A16), (A19), (A22), and (A23) are invalid. Since the principal rate of radial curvature is zero in regime AB (eq. (8)), a discontinuity in slope exists at $r = 0$.

The discontinuities in the second derivatives $\frac{\partial^2 w}{\partial r^2}$, $\frac{\partial \dot{w}}{\partial r}$, and $\ddot{w}$ which appear as one crosses from one side of the moving circle to the other can be shown to satisfy the discontinuity relationships (eqs. (10) and (11)). The velocity remains continuous, as was assumed initially (see eqs. (12) and (13)), and so does the radial slope $\partial w/\partial r$ (see eqs. (A10), (A14), and (A15)) in passing through the hinge circle. The deflection w, of course, also remains continuous. (See eqs. (26) and (28).) The discontinuity in $\partial^2 w/\partial r^2$ is given by the second term in equation (A12) (divided by $-h$ and evaluated at $\frac{r}{b} = \frac{\rho}{b}$)

which is also the negative of the discontinuity in $\partial\dot{w}/\partial r$ divided by $d\rho/dt$ (eq. (16)). The discontinuity in $\partial\dot{w}/\partial r$ is found from the difference between equations (A7) and (A8) when $\frac{r}{b} = \frac{\rho}{b}$ divided by $-h/r$; this difference, according to equation (11), equals the negative of the discontinuity in the acceleration divided by $d\rho/dt$. This result can be verified with equations (15) and (16).

REFERENCES

1. Riney, T. D.; and Heyda, J. F.: Hypervelocity Impact Calculations and Their Correlation With Experiment. Tech. Inform. Ser. No. R64SD64 (Contract No. AF 08(635)-3781), Missile Space Div., Gen. Elec. Co., Sept. 1964.

2. Becker, Karl R.; Watson, Richard W.; and Gibson, Frank C.: Hypervelocity Impact Phenomena. Bur. Mines, U.S. Dept. Interior, Apr. 5, 1962.

3. D'Anna, Philip J.; and Heitz, Roger M.: Evaluation of Self-Sealing Structures for Space Vehicle Application. NASA CR-485, 1966.

4. Lundeberg, J. F.; Stern, P. H.; and Bristow, R. J.: Meteoroid Protection for Spacecraft Structures. D2-24056(Contract NAS3-2570), Boeing Co., Oct. 1965.

5. Hopkins, H. Geoffrey; and Prager, William: On the Dynamics of Plastic Circular Plates. Z. Angew. Math. Phys., vol. 5, no. 4, July 15, 1954, pp. 317-330.

6. Wang, A. J.: The Permanent Deflection of a Plastic Plate Under Blast Loading. J. Appl. Mech., vol. 22, no. 3, Sept. 1955, pp. 375-376.

7. Wang, A. J.; and Hopkins, H. G.: On the Plastic Deformation of Built-In Circular Plates Under Impulsive Load. J. Mech. Phys. Solids, vol. 3, no. 1, Oct. 1954, pp. 22-37.

8. Perzyna, Piotr: Dynamic Load Carrying Capacity of a Circular Plate. Arch. Mech. Stosowanej, vol. 10, no. 5, 1958, pp. 635-647.

9. Florence, A. L.: Clamped Circular Rigid-Plastic Plates Under Central Blast Loading. Int. J. Solids Structures, Pergamon Press Ltd., vol. 2, no. 2, Apr. 1966, pp. 319-335.

10. Hopkins, H. G.; and Prager, W.: The Load Carrying Capacities of Circular Plates. J. Mech. Phys. Solids, vol. 2, no. 1, Oct. 1953, pp. 1-13.

11. Olszak, W.; Mróz, Z.; and Perzyna, P.: Recent Trends in the Development of the Theory of Plasticity. Macmillan Co., c.1963.

12. Prager, William: On the Use of Singular Yield Conditions and Associated Flow Rules. J. Appl. Mech., vol. 20, no. 3, Sept. 1953, pp. 317-320.

13. Mróz, Zenon: Plastic Deformations of Annular Plates Under Dynamic Loads. Arch. Mech. Stosowanej, vol. 10, no. 4, 1958, pp. 499-516.

14. Thomson, Robert G.: Plastic Deformation of Plates Subjected to a General Gaussian Distribution of Impulse. Ph.D. Thesis, Virginia Polytech. Inst., June 1966.

NASA-Langley, 1968 —— 32 L-5092

"The aeronautical and space activities of the United States shall be conducted so as to contribute . . . to the expansion of human knowledge of phenomena in the atmosphere and space. The Administration shall provide for the widest practicable and appropriate dissemination of information concerning its activities and the results thereof."

—NATIONAL AERONAUTICS AND SPACE ACT OF 1958

NASA SCIENTIFIC AND TECHNICAL PUBLICATIONS

TECHNICAL REPORTS: Scientific and technical information considered important, complete, and a lasting contribution to existing knowledge.

TECHNICAL NOTES: Information less broad in scope but nevertheless of importance as a contribution to existing knowledge.

TECHNICAL MEMORANDUMS: Information receiving limited distribution because of preliminary data, security classification, or other reasons.

CONTRACTOR REPORTS: Scientific and technical information generated under a NASA contract or grant and considered an important contribution to existing knowledge.

TECHNICAL TRANSLATIONS: Information published in a foreign language considered to merit NASA distribution in English.

SPECIAL PUBLICATIONS: Information derived from or of value to NASA activities. Publications include conference proceedings, monographs, data compilations, handbooks, sourcebooks, and special bibliographies.

TECHNOLOGY UTILIZATION PUBLICATIONS: Information on technology used by NASA that may be of particular interest in commercial and other non-aerospace applications. Publications include Tech Briefs, Technology Utilization Reports and Notes, and Technology Surveys.

Details on the availability of these publications may be obtained from:

SCIENTIFIC AND TECHNICAL INFORMATION DIVISION

NATIONAL AERONAUTICS AND SPACE ADMINISTRATION

Washington, D.C. 20546